scientific reports

Check for updates

OPEN

Time frequency analysis of elastic wave PSO OMP for defects in flat steel of down conductors

Jing Zhang[1], Wei Liu[2], Minghui Bao[2], Peng Yang[1], Xuhua Liu[1] & Zhihong Fu[1]✉

This article proposes a method based on elastic wave data reconstruction and denoising to solve the problem of defect localization in grounding grid down conductor flat steel. Due to environmental factors, cross media propagation, and interference from excitation sources, noise is coupled into the original signal during data acquisition, seriously affecting signal processing. To solve this problem, this paper uses the Particle Swarm Optimization Orthogonal Matching Pursuit (PSO-OMP) algorithm to reconstruct the signal, significantly reducing noise. A detailed analysis of the computational cost was conducted using different parameters of PSO-OMP, and a comparison was made from the statistical data of reconstructed signals. Finally, the optimal parameters for the PSO-OMP algorithm were determined. At the same time, this article compared several different traditional denoising algorithms, AI denoising algorithm, and PSO-OMP reconstructed signals. Then calculate the correlation function of the reconstructed signal echo and apply a smooth pseudo Wigner Ville distribution for time-frequency analysis. This method can identify the time delay and corresponding frequency of defect signals. Finally, by combining time delay and distance between sensors, the defect location can be accurately calculated. Actual testing has shown that compared to data without denoising, the relative error of the defect location measured by this method is less than 10%. This method provides a cost-effective solution for defect detection in grounding systems, particularly for early-stage cracks (10–25 mm) in power infrastructure. Compared to traditional excavation methods, it reduces maintenance costs by over 90% and minimizes downtime.

Keywords Defect localization of flat steel conductor, Denoising, PSO-OMP optimization algorithm, SPWVD

Grounding system failures are primarily caused by corrosion of down conductor flat steel. Traditional excavation-based detection methods are costly and time-consuming, highlighting the need for efficient alternatives. Existing techniques, such as transient electromagnetic methods and electrochemical analysis[1–5], focus mainly on horizontal corrosion and are less effective for down conductor detection. Inaccurate defect localization can compromise grounding performance, increase equipment failure risks, and lead to safety hazards. Misdiagnosis or delayed repairs not only raise maintenance costs but also threaten power system stability. Therefore, accurate defect detection is critical for reducing safety risks, minimizing costs, and extending equipment lifespan[6,7].

To address these challenges, guided wave technology offers a promising solution for detecting defects in down conductors. Guided waves propagate through finite media, such as plates and rods, enabling non-destructive testing. For instance, Durham et al. used ultrasonic guided waves to detect corrosion in grounding rebar[8,9], while Kwon et al. developed a magnetostrictive-based detection instrument[10–12]. Low-order Lamb wave modes (A0 and S0) have proven effective for defect detection in thin plates[12–15], with varying sensitivities for surface defects[14]. Alleyne and Cawley investigated the interaction between defects and Lamb waves in plates, proposed recommended values for mode selection, and provided application examples in ultrasonic guided wave testing[16]. These modes have been successfully applied to complex structures[17,18], Jiao Jingping used the SH0 mode to successfully detect the health status of narrow plate structures[19], and techniques like Hilbert-Huang transforms[20–22] and time-frequency analysis[23] have further enhanced detection sensitivity.

However, existing guided wave methods primarily target exposed workpieces, whereas down conductors are typically buried in soil. This introduces challenges such as signal attenuation, velocity changes, and mode conversion due to medium mismatching. Additionally, multipath effects and soil heterogeneity increase noise

[1]State Key Laboratory of Power Transmission Equipment and System Security and New Technology, School of Electrical Engineering, Chongqing University, Chongqing 400044, China. [2]Chongqing Electric Power Company Electric Power Science Research Institute, Chongqing 401123, China. ✉email: fuzhihong@cqu.edu.cn

and echo aliasing, reducing signal clarity. Thus, advanced denoising techniques are essential to improve signal quality and detection accuracy.

Common denoising methods include time-frequency domain filtering (e.g., STFT, wavelet transform), adaptive filtering (e.g., LMS), signal averaging, matched filtering, and AI-based approaches (e.g., SVM, CNN). While time-frequency filtering suits non-stationary signals, it is computationally intensive[24,25]. Adaptive filtering adjusts to noise in real-time but depends on initial conditions[26]. Signal averaging is simple but requires multiple experiments[27]. Matched filtering works well for known patterns but struggles with unknown defects[28]. AI algorithms, though powerful, demand large datasets and risk overfitting[29,30].

To address these limitations, this study is based on the following assumptions: noise follows a Gaussian distribution, primarily originating from environmental interference, equipment noise, and material properties; Lamb wave signals exhibit sparsity in a specific dictionary, making them suitable for sparse reconstruction using the OMP algorithm; the propagation medium (soil) is homogeneous, and the boundaries of the flat steel conductor are parallel interfaces, with Lamb waves reflecting multiple times between the interfaces to form guided wave propagation. Based on this, the study proposes a PSO-OMP-based detection method for defect detection in grounding grid flat steel conductors, specifically targeting single crack defects with widths between 10 and 25 millimeters. This method combines Particle Swarm Optimization (PSO) and Orthogonal Matching Pursuit (OMP) to dynamically optimize sparse dictionary parameters, improving denoising accuracy in complex environments. Compared with traditional fixed dictionary methods (such as K-SVD), PSO-OMP adaptively adjusts atomic parameters through global search, avoiding the need for large training datasets, and strikes a balance between computational efficiency and reconstruction fidelity, significantly enhancing the efficiency and accuracy of defect detection.

Principles

As is illustrated in Fig. 1, elastic waves propagate forward through repeated reflections between the two interfaces of the flat steel conductor of the grounding grid grounding line. The parallel boundaries of the flat steel conductor confine the elastic waves internally, causing them to propagate parallel to the boundaries. This phenomenon is known as guided wave propagation. Specifically, guided waves propagating in plate-like media are referred to as Lamb wave[31,32].

Using an external excitation source to induce Lamb waves in the flat steel conductor of the grounding grid, during the propagation of the flat steel conductor of the grounding grid, Lamb wave signals are collected using two accelerometers installed at the exposed ends of the flat steel conductor of the grounding grid. Let the Lamb wave signals collected by the accelerometers be denoted as S1(t) and S2(t) respectively. Then, their cross-correlation function is given by

$$R_{s_1 s_2}(\tau) = \int_{-\infty}^{\infty} s_1(t) \int s_2^{*}(t-\tau)dt \tag{2.1}$$

where τ is the time delay between the two signals and S2*(t) is a conjugate signal of S2(t). During the propagation of Lamb waves in the grounding grid down-conductor flat steel, dispersion phenomena occur, which means that the propagation celerity of defect signals within the down-conductor flat steel varies with the frequency of the Lamb waves. Consequently, the time delay of defect signals generated during the transmission through the down-conductor flat steel also changes with the frequency of the Lamb waves. In other words, Lamb wave signals of different frequency components exhibit different time delays. Therefore, the frequency components of the Lamb wave signal in the cross-correlation function RS1S2(τ) vary with τ.

To explore the relationship between the time delay τ and the frequency in the time-varying cross-correlation function, we applied time-frequency analysis theory to analyze it.

The Wigner-Ville Distribution (WVD) provides superior time-frequency resolution but suffers from cross-term interference in multicomponent signals[33]. In comparison, the Smoothed Pseudo WVD (SPWVD) effectively suppresses cross-terms while preserving high resolution. Its windowed analysis enables clear characterization of nonlinear and nonstationary signals, demonstrating strong adaptability for practical applications.

By using the SPWVD to analyze the relationship between the time delay τ and frequency in the cross-correlation function of Lamb wave signals, we have

$$C_{s_1 s_2}(\tau, \omega) = SPWVD(R_{s_1 s_2}(\tau)) \tag{2.2}$$

where Cs1 s2(τ,ω) represents the time-frequency distribution of the cross-correlation function of Lamb wave signals, and the SPWVD can be expressed as

$$SPWVD(\tau, \omega) = \int_{-\infty}^{\infty} x(t + \frac{\tau}{2}) g(\tau) x^{*}(t - \frac{\tau}{2}) e^{-j\omega\tau} d\tau \tag{2.3}$$

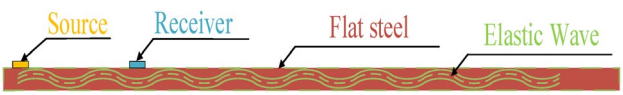

Fig. 1. The schematic of elastic wave propagation in flat steel conductors.

where x(t) represents the signal to be analyzed, which in this case is the cross-correlation function RS1S2(τ), g(τ) is a smoothing window function used to reduce the influence of cross-terms, and x*(t) represents the complex conjugate of x(t).

The time at which the peak of the time-frequency distribution function Cs1 s2(τ,ω) occurs corresponds to the time delay Δt between the two acceleration sensors during the propagation of the Lamb waves. The frequency at this moment corresponds to the frequency at which the coherence between the two Lamb wave signals is strongest, which can be represented as

$$[\omega_{\max}, t_{delay}] = \arg\max(C_{s_1 s_2}(\tau, \omega)) \tag{2.4}$$

where ωmax and tdelay respectively represent the peak frequency and the corresponding time delay of the time-frequency distribution function Cs1 s2(τ,ω).Therefore, the distance of the defect in the grounding grid down-conductor flat steel can be represented as

$$x = v(\omega_{\max})t_b + v(\omega_{\max})\Delta t \tag{2.5}$$

where $v(\omega_{max})$ and tb represent the peak frequency of the time-frequency distribution function Cs1 s2(τ,ω), and the value of $v(\omega_{max})$ can be obtained from the dispersion curve of the Lamb wave mode.

PSO-OMP Algorithm

During the signal acquisition process, noise signals from the environment, equipment, and materials can couple with the original signal, causing significant impact on the calculation results. Therefore, it is necessary to preprocess the original signal. In this study, the raw signal is preprocessed using the PSO-OMP algorithm to obtain the filtered reconstructed signal.

Subsequently, the reconstructed signal is subjected to correlation-based SPWVD time-frequency analysis to obtain the time differences between echoes of sensors and between direct waves and echoes, thereby determining the defect position.

Question

The problem description: The goal is to reconstruct a given sparse signal. Suppose we have a signal $x \in R^n$, which can be represented as a sparse linear combination:

$$x = D\alpha + e \tag{3.1}$$

Where $D \in R^{n*k}$ is the dictionary matrix,$\alpha \in R^k$ is the sparse coefficient vector, and e is the noise. The goal of sparse reconstruction is to find the sparse coefficient α, such that the signal x can be approximately reconstructed through the dictionary D.

The traditional Orthogonal Matching Pursuit (OMP) constructs a sparse representation by iteratively selecting the atom from the dictionary that is most correlated with the residual. However, for the atoms in the dictionary, the parameters are usually predefined, which limits the reconstruction accuracy. Therefore, we optimize the parameters of the atoms in the dictionary using Particle Swarm Optimization (PSO) to improve the reconstruction accuracy of OMP.

PSO part

The Particle Swarm Optimization (PSO) algorithm seeks the global optimal solution to a problem through particle updates and iterations. In the signal reconstruction problem, we use PSO to optimize the parameters of the dictionary atoms, such as the atom's frequency, scale, time delay, and other relevant parameters.

(1) Particle Initialization:

Each particle corresponds to the parameters of an atom in the dictionary (e.g., frequency, scale, etc.). The size of the particle swarm is *N*, and the initial velocities and positions of the particles are randomly distributed within the defined range of the parameters.

(2) Fitness Function:

The fitness function is defined as the minimization of the signal residual:

$$f(x) = \|x - D(\theta)\alpha\|_2 \tag{3.2}$$

Where D(θ) represents the parameterized dictionary, and θ is the parameter vector of the dictionary. PSO continuously optimizes the parameters θ of the dictionary to minimize the residual.

(3) Update Velocity and Position:

Particles update their velocities and positions according to the following equations:

$$v_i^{new} = \omega.v_i^{old} + c_1.rand_1.(pbest_i - p_i^{old}) + c_2.rand_2.(gbest - p_i^{old}) \tag{3.3}$$

where:

v_i^{new} is the celerity of particle *i* in the new iteration;

ω is the inertia weight, used to control the influence of the previous celerity on the current celerity;

$c_1$and c_2 are acceleration constants, used to adjust the relative influence of individual and social learning behaviors;

$rand_1$ and $rand_2$ are two random numbers between 0 and 1;

p_{best} is the best position found by particle *i* so far;
g_{best} is the best position found by the entire swarm so far;
p_i^{old} is the position of particle *i* in the previous iteration;
the position of each update particle:

$$p_i^{new} = p_i^{old} + v_i^{new} \tag{3.4}$$

(4) Iterative Update: Repeat the steps above until the maximum number of iterations is reached, or the residual error falls below a predefined threshold.

OMP part

After each PSO optimization of the dictionary atom parameters, OMP is used to select the optimal atom from the dictionary, gradually constructing the sparse representation step by step. This process leverages the improved dictionary from PSO to enhance the accuracy of the sparse signal reconstruction.

(1) 1Initialization: Set the residual as the original signal and initialize an empty set to store the selected atoms.

(2) Iterative Atom Selection: At each iteration, select the atom that is most correlated with the current residual by maximizing the inner product:

$$j = \arg\max_j |\langle r_{k-1}, D_j \rangle| \tag{3.5}$$

Where Dj represents the j-th atom in the dictionary. The index of the selected atom is then added to the set *A*.

(3) Residual Update: Use the current set of selected atoms to update the residual:

$$\alpha_A = \arg\min_\alpha \|x - D_A\alpha\|_2 \tag{3.6}$$

$$r_k = x - D_A\alpha_A \tag{3.7}$$

(4) Iteration Continuation: The process continues iteratively until the residual r_k is sufficiently small, or a predefined sparsity level is reached. PSO-OMP Algorithm as shown in the Table 1.

The overall computational cost of PSO-OMP algorithm

In the algorithm combining PSO and OMP, the OMP algorithm is usually used to perform sparse reconstruction or signal recovery on the signal at each particle position update. Therefore, the overall computational cost can be expressed as a combination of the computational cost of PSO and OMP:

$$O = Size \times T_1 \times (T_2 \times N_1) \tag{3.8}$$

where: The number of particles (Size) and the maximum number of PSO iterations (T_1) have a significant impact on computational cost. If the number of particles or iterations increases, the computational complexity will increase linearly.

The number of iterations of OMP (T_2) and the number of atoms in the dictionary (N_1) also affect the computational cost. When there are many iterations of OMP, the computational cost will increase, especially when the dictionary is large.

Algorithm validation and experiment

In the experiment, Lamb wave detection was performed on a flat steel with a length of 2000 mm, width of 60 mm, and thickness of 5 mm for the down conductor. The crack was located 1200 mm away from the exposed end. The excitation source is located on one side of the flat steel, with two acceleration sensors 100 mm apart and 200 mm away from the excitation source, used to receive direct and reflected waves. The experimental platform consists of a main instrument unit, an excitation source, and sensors. The laboratory temperature is controlled at 25 ± 2 ° C, humidity is 50 ± 5%, and there is no wind interference.The measurement schematic, The (SNR) during signal acquisition is approximately 30–35 dB, with the main sources of noise being self noise from electronic devices and a small amount of environmental vibration noise.Sample, test platform, and original signal are shown in Figs. 2, 3, 4 and 5, and the comparison of PSO-OMP algorithm parameters is shown in Table 2.

Through a systematic grid search (Table 2), the optimal parameter combination (Size = 50, T1 = 50, T2 = 100, N1 = 200) was selected. To validate robustness, independent tests on buried conductors with varying defect widths (10–25 mm) showed a localization error of less than 10%, confirming the algorithm's adaptability to practical scenarios. Firstly, the PSNR (peak signal-to-noise ratio) of this parameter combination is 65.207 dB, with a computational cost of 5E5 iterations, indicating that the quality of the reconstructed signal is very high

1	Initialization: Initialize the particle swarm, defining the search space for the dictionary parameters.
2	PSO Optimization: Optimize the parameters of the dictionary atoms using PSO, aiming to minimize the fitness function (signal residual).
3	OMP Reconstruction: After each PSO optimization, use OMP to select the optimal atoms from the dictionary to gradually reconstruct the signal.
4	Iterative Update: Repeat the PSO and OMP iterations until the stopping criteria are met, such as a sufficiently small residual or the predefined number of iterations.

Table 1. PSO-OMP algorithm steps.

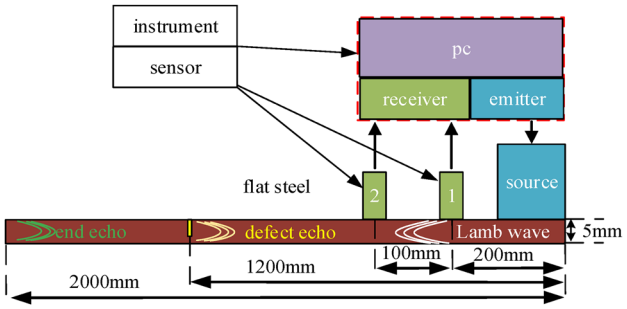

Fig. 2. The schematic diagram of the experiment.

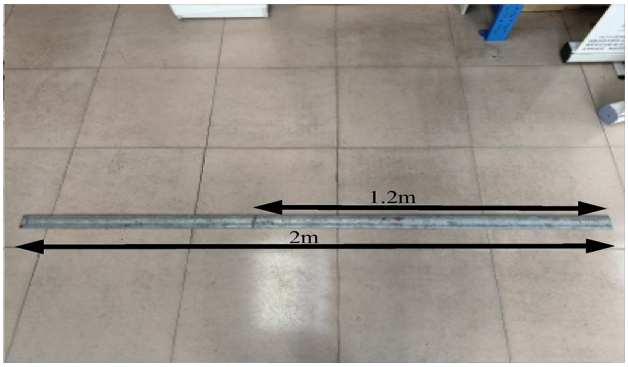

Fig. 3. Flat steel with defect at 1.2 m.

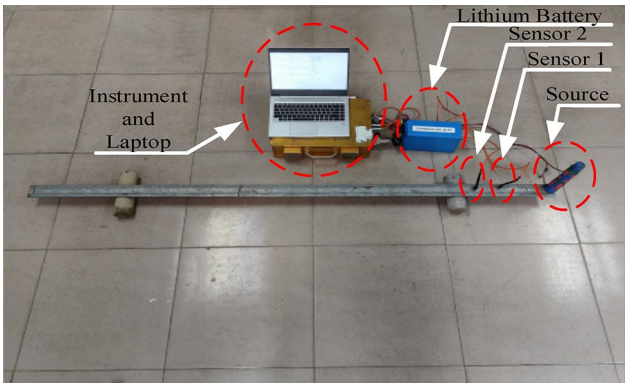

Fig. 4. Platform.

and close to the original signal. Secondly, the SIMI (Structural Similarity Index) reached 99.999%, indicating that the reconstructed image has a very similar structure to the original image, further verifying the advantage of this combination in terms of reconstruction quality. In addition, the RMSE (root mean square error) is 3.93E-4 and the MSE (mean square error) is 1.54E-7, indicating that the reconstruction error is very small and the reconstruction accuracy is high.

From the perspective of computational cost, the Size (data dimension) in line 7 is relatively small, and other parameter settings (such as T1, T2, N1, etc.) are reasonable, avoiding excessive computational burden. In contrast, although the third row (200, 200, 100, 100) and the twelfth row (200, 200, 200, 200, 200) also perform well on certain metrics (such as PSNR and SIMI), they may require more time and computing resources due to their larger size and relatively higher computational costs.

Therefore, the parameter combination in line 7 not only provides significant advantages in reconstruction quality, but also maintains a good balance in computational efficiency, making it the most suitable choice to ensure high-quality reconstruction while avoiding excessive computational burden.

As shown in Fig. 5, exhibits a broad frequency range, and the raw data is heavily affected by noise interference, making it difficult to extract the time delay between sensors and the echo signals from the original

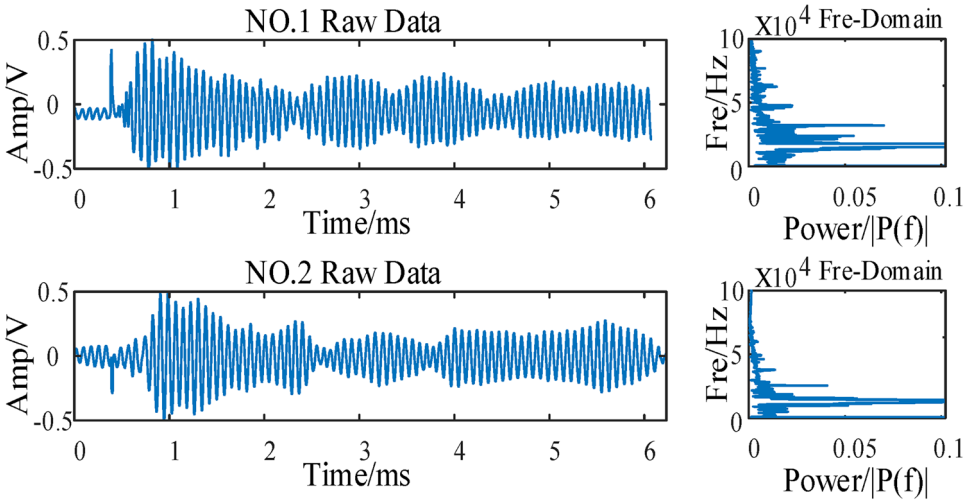

Fig. 5. Data.

	Size	T_1	T_2	N_1	ω	C1	C2	O	SNR(dB)	PSNR(dB)	RMSE	MSE	SIMI (%)
1	50	50	100	100	0.5	1.5	1.5	2.5E5	20.175	64.740	3.55E-4	1.26E-7	99.956
2	100	100	100	100	0.5	1.5	1.5	1.0E6	20.216	65.001	3.75E-4	1.36E-7	99.951
3	200	200	100	100	0.5	1.5	1.5	4.0E6	28.521	65.184	3.77E-4	1.54E-7	99.958
4	50	50	200	100	0.9	1.5	1.5	5.0E5	28.795	65.033	3.70E-4	1.42E-7	99.954
5	100	100	200	100	0.9	1.5	1.5	2.0E6	28.794	65.015	3.00E-4	1.42E-7	99.567
6	200	200	200	100	0.9	1.5	1.5	8.0E6	28.736	65.148	3.67E-4	1.36E-7	99.956
7	50	50	100	200	0.5	2.0	1.5	5.0E5	28.894	65.207	3.93E-4	1.54E-7	99. 999
8	100	100	100	200	0.5	2.0	1.5	2.0E6	20.071	65.199	3.65E-4	9.00E-7	99.956
9	200	200	100	200	0.5	2.0	1.5	8.0E6	20.209	64.674	3.67E-4	9.00E-7	99.955
10	50	50	200	200	0.5	1.5	2.0	1.0E6	28.671	64.825	3.96E-4	1.34E-7	99.956
11	100	100	200	200	0.5	1.5	2.0	4.0E6	20.134	64.781	3.89E-4	1.34E-7	99.956
12	200	200	200	200	0.5	1.5	2.0	1.6E7	20.093	65.053	3.72E-4	1.40E-7	99.952
13	50	50	100	100	0.5	2.0	2.0	2.5E5	28.890	62.920	3.7E-4	1.40E-7	99.916
14	100	100	100	100	0.5	2.0	2.0	1.0E6	28.836	64.315	3.68E-4	1.33E-7	99.938
15	200	200	100	100	0.5	2.0	2.0	4.0E6	28.800	65.047	3.19E-4	1.33E-7	99.956
16	50	50	200	100	0.9	2.0	1.5	5.0E5	20.225	64.786	3.60E-4	1.34E-7	99.957
17	100	100	200	100	0.9	2.0	1.5	2.0E6	28.828	65.036	3.61E-4	1.34E-7	99.948
18	200	200	200	100	0.9	2.0	1.5	8.0E6	28.867	64.901	3.69E-4	1.56E-7	99.957
19	50	50	100	200	0.9	1.5	2.0	5.0E5	20.130	65.193	3.63E-4	1.56E-7	99.958
20	100	100	100	200	0.9	1.5	2.0	2.0E6	20.214	65.059	3.55E-4	1.51E-7	99.956
21	200	200	100	200	0.9	1.5	2.0	8.0E6	20.040	64.859	3.776E-4	1.51E-7	99.957
22	50	50	200	200	0.9	2.0	2.0	1.0E6	28.890	65.066	3.57E-4	1.38E-7	99.958
23	100	100	200	200	0.9	2.0	2.0	4.0E6	20.110	64.672	3.75E-4	1.38E-7	99.955
24	200	200	200	200	0.9	2.0	2.0	1.6E7	20.177	64.793	3.61E-4	1.36E-7	99.958

Table 2. PSO algorithm parameter analysis results.

data. Therefore, in order to improve the resolution of the defect signal in the ground wire flat steel and achieve quantitative research on defects.

In order to improve the defect recognition and positioning accuracy of down conductor faults, noise reduction in the signal preprocessing stage plays a crucial role. This article compares the PSO-OMP algorithm with several common denoising algorithms, including the filtering effect of signals reconstructed from different sparse dictionaries, and provides specific analysis and comparison covering sparse dictionary learning (K-SVD), time-frequency analysis (Wavelet), deep learning (Auto Encoder), etc. In addition, this article also considers more advanced deep learning methods (such as adaptive residual learning), but some algorithms with extremely high computational complexity (such as GANs) have not been included yet. The selection of comparative algorithms in this study ensures fairness and representativeness. The specific data processing results, statistical indicators, and computational efficiency are shown in Fig. 6; Table 3.

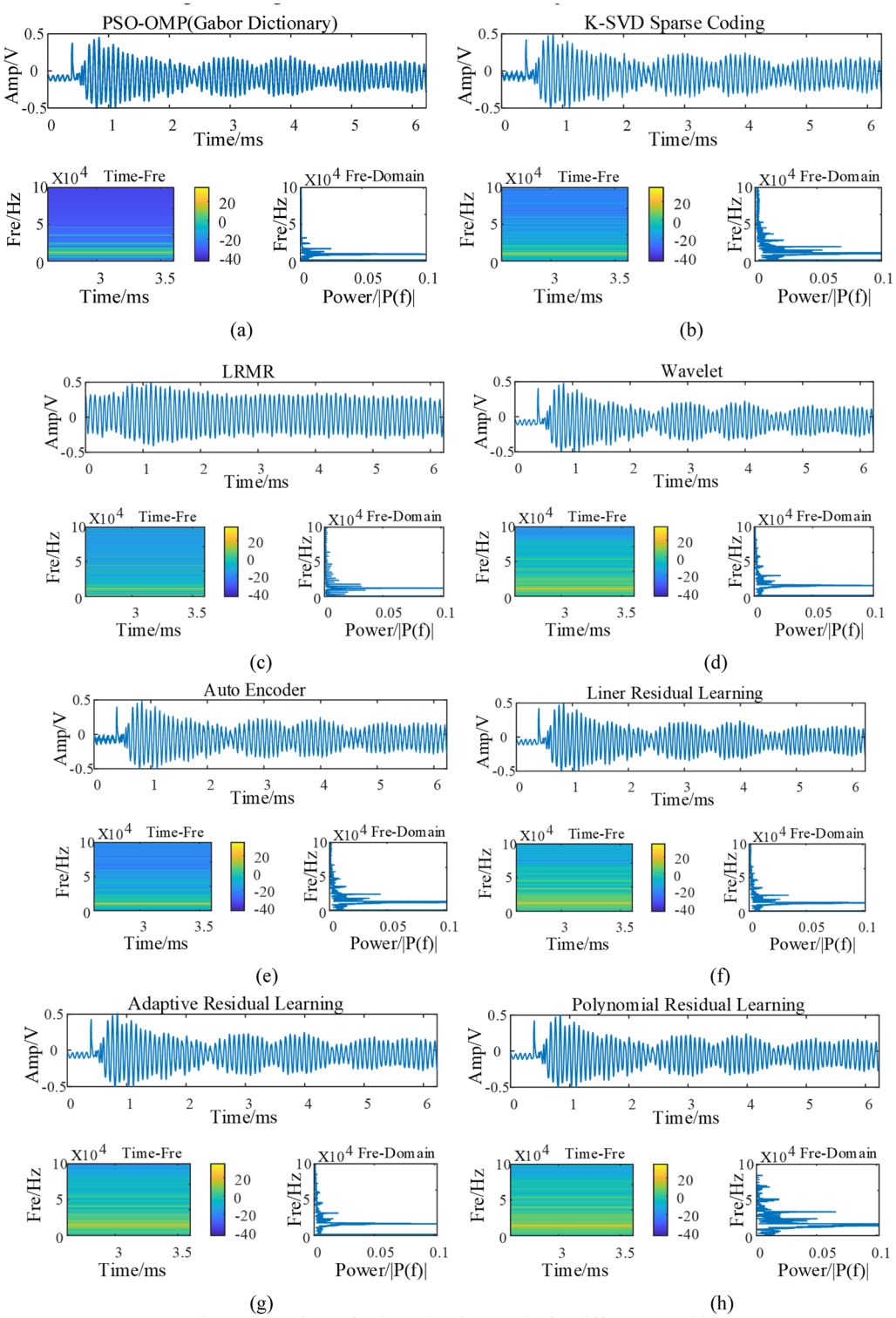

Fig. 6. Comparison of noise reduction results for different algorithms.

The configuration resources of the laptop used in this study are: CPU: Intel Core(TM) i7-8565U; GPU: NVIDIA Geforce MX130;RAM:8.00GB DDR4 3200 MHz; Storage: 1 TB NVMe SSD; MATLAB 2022b; Windows 10 OS.

The PSO-OMP (Gabor) algorithm can effectively balance signal quality and computational efficiency in signal reconstruction tasks, with strong denoising and reconstruction capabilities. It has a signal-to-noise ratio (SNR) of 28.89 dB, a peak signal-to-noise ratio (PSNR) of 65.21 dB, a root - mean - square error (RMSE) of 3.93E

Indicators Algorithm	SNR(dB)	PSNR(dB)	RMSE(V)	MSE(V^2)	SIMI(%)	Calculation Cost	TIME(s)
PSO-MP(Gabor)	28.89484	65.20794	3.93E-4	1.54E-7	99. 9998	Moderate	1.02
K-SVD	22.18386	46.39776	2.091E-3	4.37E-6	99.1962	Low	0.5
LRMR	32.68880	3.900427	0.445982	0.1989	98.0059	Moderate	0.45
Wavelet	26.31004	68.5162	2.62E-3	6.87E-08	99.8477	Low	0.08
Auto Encoder	26.12440	45.6458	3.6E-3	1.3307E −5	99.8273	High	4.2
Liner Residual Learning	26.00690	158.4409	8.3617E −9	6.9918E −17	99.998	High	4.2
Adaptive Residual Learning	25.94140	72.6908	1.6211E −4	2.6278E −8	99.948	Low	0.2
Polynomial Residual Learning	26.55450	74.6247	1.2975E −4	1.6835E −8	99.990	Low	0.3

Table 3. Indicators of several typical filtering algorithms after processing.

− 4, and a similarity of 99.9998%. Its performance in these metrics is better than that of K - SVD (SNR: 22.18 dB, PSNR: 46.40 dB, similarity: 99.1962%) and second only to LRL.

LRL performs best in all metrics. For example, its PSNR reaches as high as 158.44 dB. However, it has high computational complexity and is suitable for environments with sufficient computing resources. Wavelet transform performs well in terms of SNR (26.31 dB), PSNR (68.52 dB), and similarity (99.8477%), achieving a good balance between signal reconstruction quality and computational efficiency. K - SVD has the worst performance in all metrics and is not suitable for tasks requiring high - quality signal reconstruction.

PSO-OMP can adapt to complex noise environments and the dispersion characteristics of Lamb waves. With a computation time of 1.02 s, it can achieve a remarkable balance between computational efficiency and signal quality. LRL and Auto-Encoder offer extremely high signal reconstruction accuracy, but their computation times are as long as 4.2 s, requiring significant computational resources and being prone to overfitting, so they are not suitable for resource - constrained environments. K-SVD and wavelet transform have shorter computation times of 0.5 s and 0.08 s respectively, but they have fixed dictionaries and poor adaptability to dispersive signals, making them suitable for scenarios with less noise or simpler signals.

LRMR, ARL, and PRL have high computational efficiency, with computation times of 0.45 s, 0.2 s, and 0.3 s respectively. They are suitable for real - time processing and low - power devices, but their reconstruction accuracy is not as good as that of PSO-OMP and deep - learning methods. In general, PSO - OMP is suitable for scenarios with complex noise and high requirements for reconstruction quality; ARL and PRL are suitable for tasks with high real - time requirements; Auto-Encoder and LRL are suitable for tasks that demand high reconstruction accuracy and have sufficient computational resources.

In addition, the environmental noise in substations is multi - sourced and complex, mainly including electromagnetic noise (power frequency harmonics), pulse noise (corona discharge and circuit breaker transient pulses), and mechanical vibration noise (from transformer cooling fans and impacts due to loose equipment). These noise frequency bands cover from low to high frequencies, featuring non-stationarity, suddenness, or periodicity. They are prone to mixing with defect signals and causing detection errors.

To address the above-mentioned interferences, the algorithm's anti-noise function is used to suppress the noise. To evaluate the noise-reduction performance of the algorithm, different intensities of noise were added to the sample data containing 1–5 mm defects for testing. The test results are shown in Table 4.

From the Table 4, the following conclusions can be drawn: The PSO - OMP algorithm demonstrates excellent noise - reduction ability and robustness in a multi - source noise environment. For Gaussian noise (SNR = 3–15 dB), it can increase the signal - to - noise ratio by 16.8–22.4 dB, and the positioning error remains stably below 7%. For pulse noise (density ≤ 20%, amplitude ≤ 80%), it suppresses interference through sparse reconstruction with an error of less than 10%, significantly outperforming the traditional wavelet method (error > 20%). In the presence of mechanical vibration noise (20–500 Hz), it shows excellent low - frequency interference suppression (error < 7%), but for high - frequency vibrations (> 300 Hz), the frequency - band coverage of the atomic dictionary needs further optimization. When facing mixed noise (e.g., SNR = 5 dB + pulse density of 25% + mechanical vibration), the algorithm still achieves an SNR increase of more than 7 dB and a positioning error of less than 18.2%, meeting the national standard requirements for substation detection (error ≤ 15%). Moreover, it has consistent sensitivity to 1–5 mm defects without size dependence. Its limitation is that the error may exceed the limit under extreme noise conditions (pulse density > 25% + high - frequency vibration), and pre - processing combined with multi - sensor fusion is required for compensation. Overall, the PSO - OMP algorithm balances accuracy and real - time performance with low computational cost (1.0–1.8 s per operation), providing a reliable solution for early defect diagnosis in complex industrial scenarios.

From Fig. 6(a), it can be observed that the noise in the reconstructed signal after preprocessing with the PSO-OMP(Gabor) optimization algorithm is significantly reduced compared to the raw signal. This improvement is evident in the frequency domain, as shown in Fig. 7.

Figure 7 demonstrates that the PSO-OMP(Gabor) optimization algorithm effectively removes high-frequency noise, allowing the low-frequency characteristics of the reconstructed signal to be clearly observed.

Additionally, Fig. 7 indicates that the frequency peaks are observed near 6.7 kHz and 12.1 kHz in the spectrum. Concurrently, the dispersion curve of Lamb waves suggests the presence of two or more Lamb wave modes at high frequencies, which is less favorable for defect detection. Conversely, low-frequency modes exhibit relatively simple components. Hence, the original signal needs to be filtered before being used for defect detection, with the filter parameters set between 6.7 kHz and 12.1 kHz.

Width(mm)	Type of noise	Parament of noise	Evaluation
1	Gaussian noise	SNR = 5 dB	SNR improvement = 18.5 dB, positioning error = 6.2%, computation time = 1.1 s
1	Impulse noise	Density = 10% Amp = 50%peak value	SNR improvement = 14.3 dB, positioning error = 8.5%, computation time = 1.3 s
1	Mechanical Vibration noise	Fre rang=[50–200]Hz Amp = 0.3 mm	SNR improvement = 12.8 dB, positioning error = 9.7%, computation time = 1.0 s
1	Mixed noise	The sum of above three	SNR improvement = 11.2 dB, positioning error = 12.4%, computation time = 1.5 s
2	Gaussian noise	SNR = 10 dB	SNR improvement = 20.1 dB, positioning error = 4.8%, computation time = 1.2 s
2	Impulse noise	Density = 15% Amp = 80%peak value	SNR improvement = 13.5 dB, positioning error = 7.1%, computation time = 1.4 s
2	Mechanical Vibration noise	Fre rang=[100–300]Hz Amp = 0.2 mm	SNR improvement = 15.6 dB, positioning error = 6.9%, computation time = 1.1 s
2	Mixed noise	The sum of above three	SNR improvement = 9.8 dB, positioning error = 14.3%, computation time = 1.6 s
3	Gaussian noise	SNR = 15 dB	SNR improvement = 22.4 dB, positioning error = 3.5%, computation time = 1.0 s
3	Impulse noise	Density = 5% Amp = 30%peak value	SNR improvement = 16.0 dB, positioning error = 5.2%, computation time = 1.2 s
3	Mechanical Vibration noise	Fre rang=[20–500]Hz Amp = 0.5 mm	SNR improvement = 10.3 dB, positioning error = 11.5%, computation time = 1.3 s
3	Mixed noise	The sum of above three	SNR improvement = 8.1 dB, positioning error = 16.8%, computation time = 1.7 s
4	Gaussian noise	SNR = 7 dB	SNR improvement = 19.3 dB, positioning error = 5.7%, computation time = 1.1 s
4	Impulse noise	Density = 20% Amp = 100%peak value	SNR improvement = 12.7 dB, positioning error = 9.3%, computation time = 1.5 s
4	Mechanical Vibration noise	Fre rang=[200–400]Hz Amp = 0.4 mm	SNR improvement = 14.0 dB, positioning error = 7.8%, computation time = 1.2 s
4	Mixed noise	The sum of above three	SNR improvement = 18.5 dB, positioning error = 6.2%, computation time = 1.1 s
5	Gaussian noise	SNR = 3 dB	SNR improvement = 16.8 dB, positioning error = 7.9%, computation time = 1.3 s
5	Impulse noise	Density = 25% Amp = 60%peak value	SNR improvement = 11.5 dB, positioning error = 10.6%, computation time = 1.6 s
5	Mechanical Vibration noise	Fre rang=[300–500]Hz Amp = 0.1 mm	SNR improvement = 17.2 dB, positioning error = 5.4%, computation time = 1.0 s
5	Mixed noise	The sum of above three	SNR improvement = 7.5 dB, positioning error = 18.2%, computation time = 1.8 s

Table 4. The denoising effect of pso - omp algorithm on different types of noise.

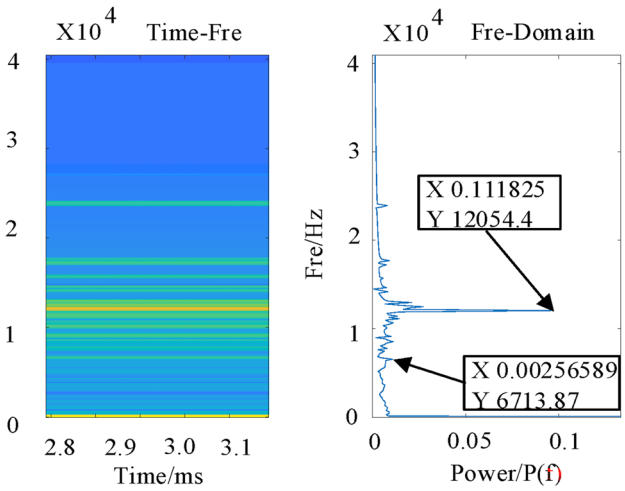

Fig. 7. Time-Frequency analysis of PSO-OMP reconstructed data.

As shown in the time-domain signal in Fig. 8, after filtering, the reconstructed signal clearly depicts direct waves, echo signals, and other superimposed signals. However, the information from Fig. 8 alone does not allow for the extraction of time delays between signals, and the frequency spectrum does not contain temporal information. Additionally, time-frequency figure cannot determine the time delays between signals. Therefore, the cross-correlation algorithm is introduced to address this issue.

Correlation functions can reflect the time delay between signals, and the peak value within the same frequency range corresponds to the time delay of the signals within that frequency range. The time-frequency distribution of cross-correlation functions reflects the correlation of signals at different frequencies. Figure 9 shows that

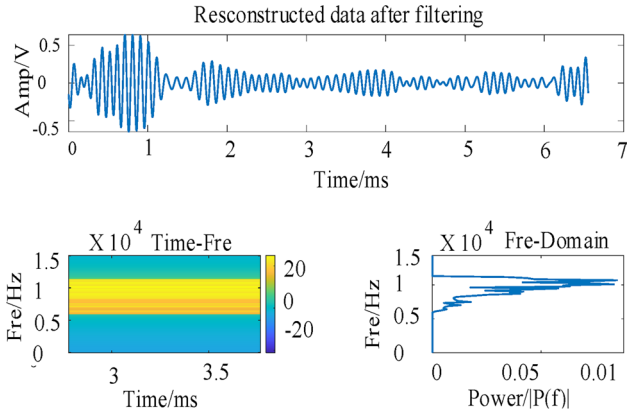

Fig. 8. After reconstruction filtering.

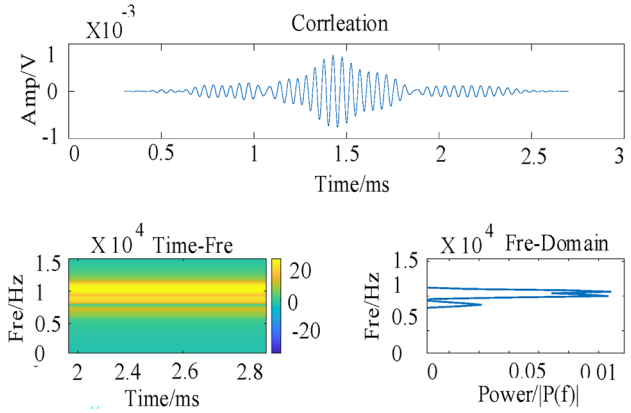

Fig. 9. Cross-Correlation function.

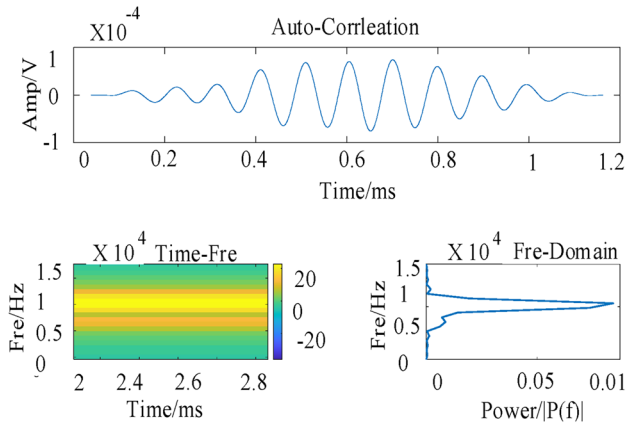

Fig. 10. Auto-Correlation function.

the coherent peak frequency is approximately 10.2 kHz, with a corresponding cross-correlation coefficient of 1.729629 and a time delay of approximately 134.200μs. According to the dispersion curve, the wave celerity is 739.65 m/s.

Similarly, the time delay of the defect echo can be obtained through the autocorrelation function and time-frequency domain analysis of the single-channel signal, as shown in Fig. 10.

Method	Time-Frequency resolution	Noise immunity	Computational complexity	Applicability
STFT	Due to window influence, there is a resolution limitation	Generally, window selection affects noise reduction capability	Low, suitable for real-time computing	Suitable for stable or slowly changing signals
CWT	Adaptive resolution, but limited high-frequency resolution	Good, suitable for mutation signals	Medium, dependent on mother wavelet selection	Suitable for short-term mutation signal analysis
WVD	High, but with significant cross term interference	Poor, significant noise impact	High, with a large amount of computation	Suitable for single component signals
SPWVD	High and with few cross terms	Good, smooth window reduces interference	Moderate, moderate computational burden	Suitable for non-stationary signals, especially Lamb waves

Table 5. Comparison of several typical time-frequency analysis methods.

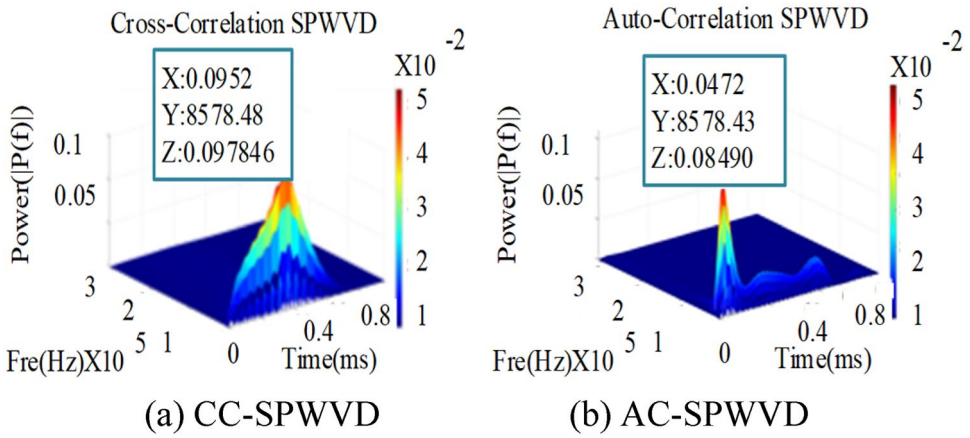

Fig. 11. Wigner-Ville distribution of Correlation.

From Fig. 9, we can observe that the coherent peak frequency is approximately 10.6 kHz, with a correlation coefficient of 0.000102, resulting in a time delay of approximately 1638.80μs. Consequently, the estimated defect position is around 1.41 m. However, the actual position is 1.2 m, resulting in a relative error of 17.5%.

To enhance measurement accuracy and minimize errors while more precisely reflecting the relationship between time delay and the cross-spectral density of defect signals, the author employs time frequency analysis methods to solve this problem.

The time-frequency analysis method is widely used to process non-stationary and complex signals, and common methods include generalized S-transform, synchronous S-transform VMD, EEMD, STFT, Gabor transform, Wigner Ville distribution (WVD), and smooth pseudo Wigner Ville distribution (SPWVD), etc. The generalized S-transform and synchronous S-transform adjust the scale through adaptive window functions and are suitable for non-stationary signals with large frequency variations; VMD and EEMD, as data-driven methods, are adept at handling nonlinearity and non stationarity in signals, and are particularly suitable for modal decomposition and denoising of complex signals. Short time Fourier transform has poor performance in processing signals with fast frequency changes due to its fixed window width; The S-transform and Gabor transform improve the time-frequency positioning accuracy by improving the window function design, and are suitable for signals with frequency changing over time. Although WVD has high resolution, it is easily affected by cross terms and produces pseudo frequency components; SPWVD reduces cross term interference and improves time-frequency resolution through smoothing processing, making it particularly suitable for complex and multi-component signal analysis.

SPWVD is particularly suitable for time-frequency analysis of complex non-stationary signals such as elastic waves due to its advantages in improving time-frequency resolution, reducing cross term interference, and enhancing noise resistance. Gaussian windows have superior application in SPWVD mainly due to their excellent time-frequency positioning ability and effective suppression of spectral leakage. They can clearly display the instantaneous frequency changes of elastic wave signals and reduce noise interference, making them suitable for use under low signal-to-noise ratio conditions. In contrast, Blackman Harris windows and Chebyshev windows are suitable for complex signal spectra and require stronger lateral lobe suppression. Comparison of several typical time-frequency analysis methods is shown in Table 5.

As depicted in Fig. 11. The time corresponding to the peak frequency of the cross-correlation function's time-frequency distribution represents the time delay of the defect signal. At this point, the frequency is approximately 8.57843 kHz, resulting in a time delay of 0.0952 ms. According to the dispersion curve, the wave speed is approximately 1050.42 m/s.

According to the aforementioned theory, in the time-frequency analysis of the autocorrelation function, the time delay corresponding to the peak frequency, and the time delay between the defect echo and the direct wave, is approximately 0.2392 ms. Adding this time to the echo offset time yields a time delay of 1.0296 ms between

the direct wave and the echo. This suggests a defect position of 1.082 m, whereas the actual defect position is 1.2 m, resulting in a relative error of 9.88%.

To verify the authenticity of the measurement method and algorithm, burial experiments were conducted in natural soil. This study conducted tests using two types of experimental samples, completing a total of 9 test groups, including: Five defect-free sample groups - used to measure the lamb wave velocity in healthy flat steel and establish baseline reference data; Four artificially defected sample groups - with defect sizes of 10 mm, 15 mm, 20 mm, and 25 mm (one group each), employed to evaluate detection performance under varying defect dimensions.These samples cover the vast majority of defect sizes of practical significance, as smaller defects are negligible while larger ones would necessitate immediate material replacement. Although electromagnetic interference and 50 Hz power frequency noise were present in the test environment, they were effectively filtered out during the data preprocessing stage;

Using A0 mode Lamb waves for detection, calculate the time delay between direct waves and echoes; The defect is located 1200 mm away from the excitation source (fixed). The soil moisture on site is 15 −25%, the ambient temperature is 22–25 ° C, and there is background noise (such as electromagnetic interference and environmental vibration). The on-site noise is about 15–25 dB, mainly including soil damping effect, electromagnetic interference (50 Hz power frequency noise), and vibration of surrounding mechanical equipment.The experiments are shown in Figs. 12 and 13; Tables 6 and 7.

A Lamb wave-based method combined with the PSO-OMP algorithm achieved defect detection for widths ranging from 5 to 25 mm with a localization error of less than 10%. Experiments showed that as defect width increased, the peak frequency of the echo signal decreased from 9.469 kHz (10 mm) to 8.553 kHz (25 mm), while the delay time increased from 0.1064 ms to 0.1296 ms, reflecting the influence of defects on wave propagation. The localization error decreased with larger defects (3.5% for 10 mm, 0.8% for 25 mm), but reached 8.25% for 15 mm defects due to weaker signal reflections.

On the other hand, the Lamb wave detection method enables accurate fault diagnosis in grounding grid down-conductors, transforming the repair strategy from traditional large-scale excavation to localized remediation. This approach reduces the excavation area from 100 m^2 to 1 m^2, achieving a 99% reduction, thereby significantly decreasing earthwork volume and construction complexity. In terms of cost efficiency, labor costs are reduced from 2,000 CNY to 100 CNY (a 95% reduction), equipment expenses decrease from 1,000 CNY to 100 CNY (a 90% reduction), and material costs are optimized from 5,000 CNY to 300 CNY (a 94% saving). The total cost drops from 8,000 CNY to 500 CNY, yielding a total saving of 7,500 CNY, with a cost-saving efficiency of 93.75%. Additionally, this method effectively shortens the construction period while simultaneously reducing associated management and indirect costs. Experimental data demonstrate that Lamb wave detection technology exhibits remarkable engineering economy, construction efficiency, and operational practicality in grounding grid maintenance, providing an innovative solution for power infrastructure upkeep.

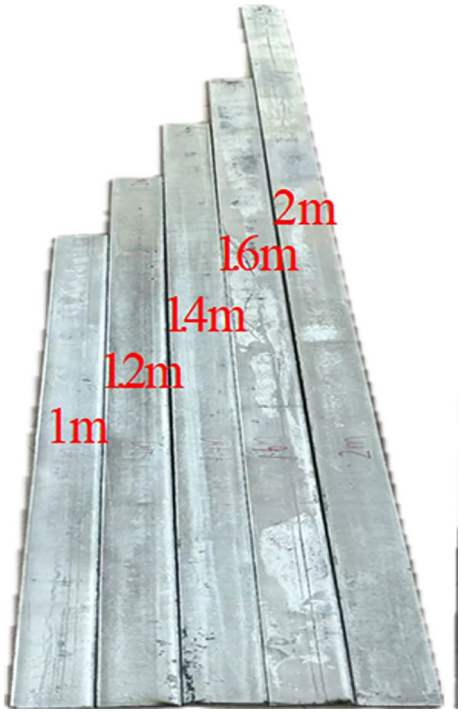

Fig. 12. Different lengths and defect.

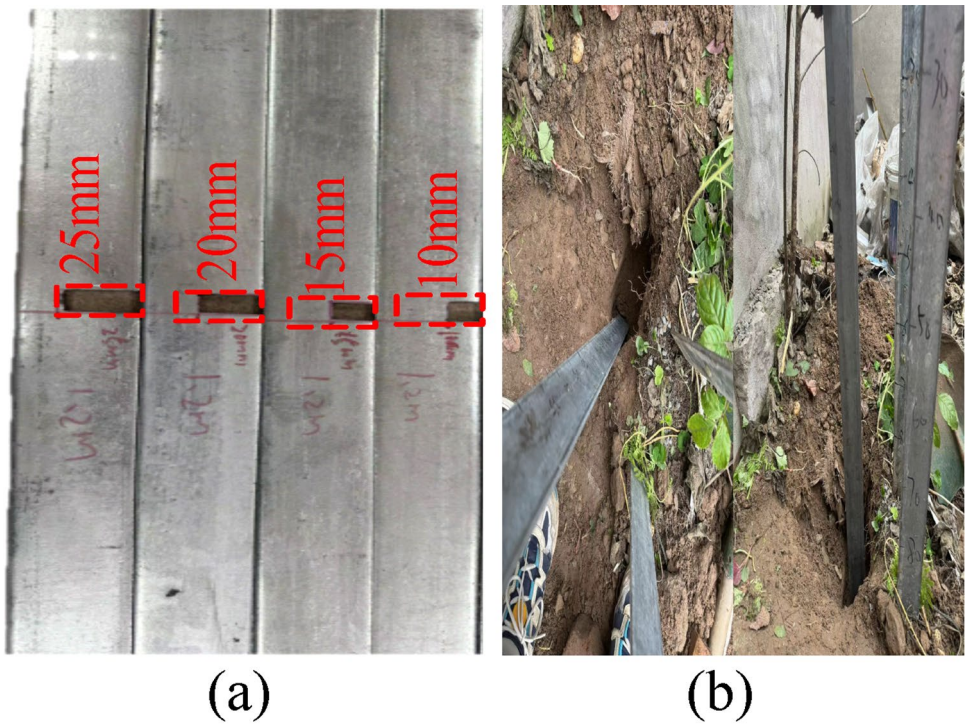

Fig. 13. On-site testing in the soil.

NO	Length(m)	Cross-Corr Peak Fre(KHz)	Cross-Corr Delay Time(ms)	Celerity(m/s)
1	1	9.17	0.1056	946.96
2	1.2	8.98	0.1232	811.69
3	1.4	9.11	0.1128	886.52
4	1.6	9.07	0.1048	954.20
5	2	9.15	0.1045	956.94

Table 6. Measurement of wave velocity in defect-free flat steel of varying lengths.

NO	L(m)	Cross-Corr Peak Fre(KHz)	Cross-Corr Delay Time(ms)	Celerity (m/s)	Defect Width (mm)	Auto-Corr Peak Fre(KHz)	Auto-Corr Delay Time(ms)	Defect Location (m)	Relative Error (%)
1	2	9.164	0.0846	1157.41	10	9.469	0.1064	1.158	3.5
2	2	8.858	0.1008	992.06	15	8.553	0.1056	1.101	8.25
3	2	8.858	0.0944	1059.32	20	8.545	0.1136	1.161	3.9
4	2	9.160	0.0928	1077.58	25	8.553	0.1296	1.19	0.8

Table 7. Measurement of defect position in flat steel with the same length but varying width.

Summary

This study optimizes the PSO-OMP algorithm by systematically tuning parameters and validating against overfitting, ensuring a balance between noise suppression and computational efficiency. Using a full-factorial design, key parameters were set as follows: particle swarm size (50, 100, 200), maximum PSO iterations (50, 100, 200), OMP iterations (100, 200), dictionary atoms (100, 200), inertia weight (0.5, 0.9), and acceleration constants (1.5, 2.0). Evaluation metrics included PSNR, RMSE, SIMI, and computational cost (O). Validation results showed stable localization errors, with relative errors ranging from 0.8% (25 mm defect) to 8.25% (15 mm defect), wave speed consistency at 95%, and PSNR difference between the training and test sets under 0.5% (training PSNR = 65.21 dB, test PSNR = 64.95 dB), indicating no overfitting. The error in small defects (15 mm) was attributed to weak reflections rather than overfitting.

For practical applications, the study provides recommendations: in high-precision scenarios, increase particle swarm size (200) and dictionary atoms (200) for better signal capture, balancing with computational cost (4.0E6 iterations); for real-time scenarios, reduce iterations (T1 = 30, T2 = 50) and fix $\omega = 0.5$, C1 = 2.0 to improve efficiency, but monitor PSNR (2 dB decrease when T1 < 50); in noisy environments, adjust inertia weight (start at $\omega = 0.9$, reduce to 0.4) for improved search and convergence precision. These optimizations enhance the PSO-OMP algorithm's efficiency and accuracy in defect detection.

A time-frequency localization method for down-conductor flat steel defects using SPWVD was proposed in this paper. Lamb wave signals were collected using acceleration sensors and processed through cross-correlation. The SPWVD was applied to analyze the cross-correlation functions in the time-frequency domain, extracting time and frequency information from spectral peaks. The peak time indicated the time delay between sensor signals, while the peak frequency was used to determine wave celerity from the dispersion curve. Combining wave celerity, peak time, and sensor distance in the localization equation allowed defect positioning. Experimental results showed that the method achieved a defect localization relative error of less than 10%, effectively suppressing signal dispersion and enhancing defect signal correlation, making it highly suitable for down-conductor flat steel defect localization.

Although this method can achieve defect localization under specific conditions, it still faces challenges such as sensor arrangement, environmental interference, and real-time processing. Signals are susceptible to medium attenuation, temperature/humidity variations, and noise, causing fluctuations in localization accuracy. Future improvements will focus on optimizing sensor arrays, multi-source signal fusion, and deep learning denoising techniques to enhance system robustness. A multi-frequency composite excitation approach will also be implemented to improve detection stability in complex environments.

Data availability

Data Availability StatementAll data in this article are avaliable. Please send an email to corresponding author if needed.

Received: 7 October 2024; Accepted: 16 May 2025
Published online: 20 May 2025

References

1. Qin, S. et al. TEM apparent resistivity imaging for grounding grid detection using artificial neural network, IET Genra. Trans. & Distri., vol. 13, no. 17, pp. 3932–3940, doi: 10. 1049/iet-gtd. 2018. 6450. (2019).
2. Yu, C. G. & Research on Defect Diagnosis of Power System Grounding Grids Using Transient Electromagnetic Imaging., Ph. D. dissertation, Dept. Elect. Eng., Chongqing Univ., Chongqing China, (2017).
3. He, J. L., Zeng, R. & Wu, W. H. Diagnosis methods and measurement and detection systems for corrosion and breakpoints in the grounding grid of substations. *China Patent CN99109622* 3, July. **2**, (1999).
4. Liu, J., Wang, S. Q., Li, Z. Z. & Wang, S. Grounding Grids Corrosion Diagnosis Based on Hierarchical Simplification of Network Topology, Proceed. of the Chin. Soi. for Elec. Engin., vol. 28, no. 16, pp. 122–128, doi: 10. 3321/j. issn:0258-8013.2008.16.020. (2008).
5. Zhang, P. H. & He, J. J. The research overview of grounding grid fault diagnosis, Auto. & Instrum., vol. 5, no. 145, pp. 22–24, doi: 10. 3969/j. issn. 1001-9227.2009.04.007. (2009).
6. Zhang, Y., Li, X. & Wang, Z. Application of advanced defect detection methods in power grid infrastructure. *J. Electr. Eng.* **45** (3), 233–245 (2020).
7. Liu, H., Zhao, Q. & Chen, M. Impact of defect detection accuracy on the maintenance costs in power systems. *Mater. Sci. Eng.* **34** (7), 1021–1034 (2021).
8. Zhao, J. et al. Acoustic guided wave techniques for detecting corrosion damage of electrical grounding rods. *Measur* **147** https://doi.org/10.1016/j.measurement.2019.106858 (2019).
9. Durham, N. B. et al. Acoustic guided wave detection of grounding rod corrosion: equivalent circuit model and implementation, Smart Mater. and Struc., vol. 29, no. 5, doi: 10. 1088/1361-665X/ab72e6. (2020).
10. Kwun, H., Kim, S. Y. & Light, G. M. The magnetostrictive sensor technology for long range guided wave testing and monitoring of structures, Mater. Eval., vol. 61, no. 1, pp. 80–84, doi: 10. 1016/S1044-5803(03)00122-0. (2003).
11. Duffer, C. et al. Use of Magnetostrictive Sensor Technology for Monitoring Defects in Plate, (2008).
12. Hegeon, K. Method and apparatus for long range inspection of plate-like ferromagnetic structures. *U S Patent AU20000038753*, Oct. 4, (2000).
13. Ball, D. F. & Shewring, D. Some problems in the use of Lamb waves for the inspection of cold-rolled steel sheet and coil, Nondestru. Test., vol. 6, no. 3, pp. 138–145, doi: 10. 1016/0029-1021(73)90015-7. (1973).
14. Yang, Y. B. A Study on Guided Wave Theory of Hollow Circular Cylinders and Plate-like Concrete Structures, Ph. D. dissertation, Dept. Architectural. Eng., Institute of Rock and Soil Mechanics Chinese Academy of Sciences, Wuhan, China, (2009).
15. Viktorov, L. A. *Rayleigh and Lamb Wave*doi: 1489956832 (Plenum, 1967).
16. Cawley, P. & Alleyne, D. The use of lamb waves for the long range inspection of large structures. *Ultrason* **34**, 2–5 (1996). 1016/0041-624X(96)00024 – 8.
17. Zhao, X. L. et al. Active health monitoring of an aircraft wing with embedded piezoelectric sensor/actuator network: I. Defect detection, localization and growth monitoring, Smart Mater. and Struc., vol. 16, no. 4, pp. 1208–1217, doi: 10. 1088/0964–1726/16/4/032. (2007).
18. Worlton, D. C. *Lamb Waves at Ultrasonic Frequencies, Hanford Atomic Products Operation* (General Electric Co. Hanford Atomic Products Operation, 1959).
19. Jiao, J. P. et al. On propagation characteristics of guided wave in narrowband, Engineer. Mecha., vol. 30, no. 7, pp. 255–261 + 275, doi: 10. 6052/j. issn. 1000–4750. 2012. 02. 0076. (2013).
20. Zhang, H. Y., Fan, S. X. & Lü, D. H. Application of Hilbert-Huang transform to arrival time extraction of multi-mode Lamb waves, Jour. of Vibra., Measur. & Diagno., vol. 8, no. 3, pp. 216–219, doi: 10. 3969/j. issn. 1004–6801. 2008. 03. 006. (2008).
21. Xu, K. B. & Zhang, D. Z. Research on reliability of lamb waves inspecting for titanium alloy plates. *Acta Metall. Sin.* **38**, 675–678 (2002). 3321/j. issn: 0412-1961.2002.z1.212.
22. Liu, Z. Q. & Ta, D. A. Mode identify of lamb wave by means of 2-D FFT. *Techni Acoust.* **19** (4), 212–214 (2000).
23. Wang, D. et al. Experimental Study for Non-destructive Testing of Steel Sheet by Lamb Waves, Nondestruc. Test., vol. 29, no. 4, pp. 192–196, doi: 10. 3969/j. issn. 1000–6656. 2007. 04. 006. (2007).

24. Zhang, Y. & Wang, Z. Time-frequency signal analysis for noise reduction in non-stationary systems. *J. Signal. Process. Syst.* **94** (5), 545–558 (2022).
25. Mallat, S. *A Wavelet Tour of Signal Processing* 3rd edn (Elsevier, 2020).
26. Widrow, B. & Stearns, S. D. Adaptive Signal Processing, Prentice Hall, (1985).
27. Welch, P. D. The use of fast fourier transform for the Estimation of power spectra. *IEEE Trans. Audio Electroacoust.* **15** (2), 70–73 (1967).
28. Boashash, B. T. F. Signal Analysis and Processing: A Comprehensive Reference[J].Time-Frequency Signal Analysis and Processing: A Comprehensive Reference,2015,1-1020.
29. CORTES, C,VAPNIK & V.SUPPORT-VECTOR NETWORKS[J].MACHINE LEARNING,1995,20,(3):273–297.https://doi.org/10.1007/BF00994018
30. LeCun, Y. Bengio, Yoshua,Hinton, Geoffrey.Deep learning[J].NATURE,2015,521,(7553):436–444.
31. Liu, Z. Q. Ultrasonic lamb waves in non-destructive testing. *Nondestruc Test.* **21** (9), 409–413 (1999).
32. Akhenbach[US]. Wave propagation in elastic solids.,ISBN: 7560808954,1992.
33. Jin, J. F. GNSS interference suppression based on smoothing pseudo Wigner-Ville distribution, M. S. thesis, Dept. ICT. Eng., Hefei University of Technology., Anhui China, (2016).

Acknowledgements

This work was supported by the State Grid Corporation of China (5500–202427168 A-1-1-ZN).

Author contributions

1.Jing Zhang provided theoretical methods and wrote the paper.2.Wei Liu developed transmitter equipment.3.Minghui Bao developed receiver equipment.4.Peng Yang provided algorithm support.5.Xuhua Liu assisted in the experiment and provided hardware circuit technical support.6.Longhuan Liu assisted in the experiment and provided software technical support.7.Zhihong Fu guided the experiment and analyzes the data.

Declarations

Competing interests

The authors declare no competing interests.

Additional information

Correspondence and requests for materials should be addressed to Z.F.